

Dispersion and dipole activity of surface phonons on Si(111) 2×1

O. L. Alerhand* and E. J. Mele

Department of Physics, University of Pennsylvania, Philadelphia, Pennsylvania 19104-6396

(Received 13 August 1987)

Using an empirical tight-binding theory for structural energies we study vibrational excitations on the π -bonded chain model of the Si(111) 2×1 surface. We calculate the phonon spectrum of the surface and find a number of modes that have the form of elementary vibrational excitations of the zigzag chains of surface atoms of the reconstructed surface. In the acoustic part of the spectrum a strong phonon-energy renormalization effect generated by electronic transitions causes an unusual softening of the Rayleigh wave at the zone boundary; this result is consistent with recent He-atom scattering experiments. We also calculate the linearized response of the charge density to lattice displacements, which we use to obtain the phonon-assisted contribution to the surface conductivity. A longitudinal-optical phonon along the surface zigzag chains generates a very large dynamic charge ($\sim 0.75e$) and is assigned to the anomalously strong dipole-active surface phonon that has been observed experimentally by high-resolution electron-energy-loss spectroscopy.

I. INTRODUCTION

In this paper we present results of theoretical studies of the lattice dynamics of the Si(111) 2×1 surface, including an expanded discussion of results we have previously reported in short communications.^{1,2} The Si(111) 2×1 surface has been one of the most-studied semiconductor surfaces, and is regarded today as one of the best understood; it remains, however, the subject of intense research. As a unified picture of the structure of the surface has emerged, the focus of attention has shifted to questions regarding excitations and dynamical properties. Our understanding of the reconstruction of the Si(111) 2×1 surface is based on Pandey's π -bonded chain model.³ According to this model the surface reconstructs by forming strongly bonded zigzag chains of surface atoms that run parallel to each other. The period doubling of the reconstruction is along the $\langle 11\bar{2} \rangle$ direction, one of three equivalent directions of the bulk terminated surface, and the surface chains run parallel to $\langle 1\bar{1}0 \rangle$ (see Fig. 1). Each surface atom has one dangling bond, and the atoms along a surface chain are inequivalent. The chains are tilted with one of the two surface atoms in the unit cell farther from the surface than the other, that is, there are up and down atoms; the up atoms are uniquely determined by the subsurface.⁴ The chain geometry of the reconstructed surface is different from the bulk terminated surface, as evidenced by the appearance of five- and sevenfold rings, compared with the sixfold rings of crystalline bulk Si. Whereas atoms along a surface chain are first nearest neighbors, and indeed they are very strongly bonded, the separation between surface atoms on neighboring chains is large; the quasi-one-dimensional character of these strongly bonded surface zigzag chains determines many of the properties of the surface. Extensive theoretical^{3,4} and experimental evidence supports the chain model as the correct model for the reconstruction of the Si(111) 2×1 surface. Among the experimental results are direct measurements

of the surface structure using scanning tunneling microscopy^{5,6} (STM) and medium-energy ion scattering⁷ (MEIS), low-energy electron diffraction (LEED) experiments,⁸ measurements of the dispersion of the surface electron bands using angle-resolved photoemission spectroscopy^{9,10} (ARPES) (it was these measurements that originally motivated Pandey to propose the chain model) and inverse ARPES,^{11,12} electron energy-loss spectroscopy (EELS) of electronic¹³ and vibrational properties,¹⁴ and optical measurements of the surface-state optical absorption.¹⁵

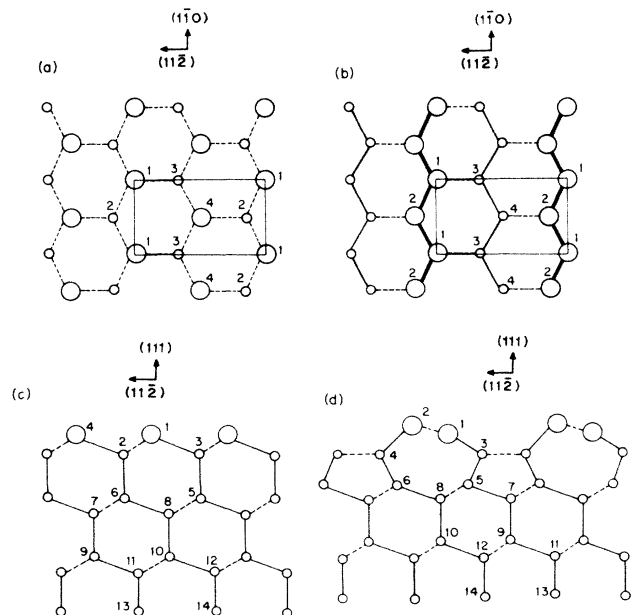


FIG. 1. (a) Top and (c) side view of the bulk-terminated Si(111) surface; (b) top and (d) side view of the π -bonded chain model. Large circles represent surface atoms, and small circles subsurface atoms.

The two most important features of the chain reconstruction are (1) the formation of the surface-chain geometry itself, and (2) the strong interaction, mostly through π bonding, between the first-nearest-neighbor surface atoms along the surface zigzag chains. As a consequence of these, the bonding along the surface chains is very strong and the surface electrons then tend to delocalize along the chains. On the other hand, the chains are quite separated from each other. Thus the surface electrons behave as nearly free electrons along the chains, but have almost no interchain coupling. These observations are confirmed by the dispersion of the electronic surface bands, which show strong dispersion along the chain direction with a small gap at the zone edge, and much weaker dispersion in the direction across the chains (see Fig. 2). The delocalization of the surface electrons along the chains reduces their kinetic energy, stabilizing the chain reconstruction of the surface.

The surface-chain geometry and the quasi-one-dimensional behavior of the surface electrons suggest the possibility for the appearance of interesting vibrational excitations on this surface. We have calculated the phonon spectrum of the surface and the dynamic charges generated by these phonons, which we use to calculate the phonon-assisted contribution to the surface conductivity. We find that the surface-phonon spectrum includes a number of modes that have the form of elementary vibrational excitations of the surface chains. Among them there is a longitudinal-optical (LO) phonon along the surface chains which generates an extremely large dynamic charge and completely dominates the phonon absorption spectrum of the surface. We assign this mode to the anomalously strongly dipole active surface phonon first observed by Ibach in 1971 in EELS experiments.¹⁶ The LO mode of the surface chains has the novel property that the dynamical dipole it generates is parallel to the surface, in apparent disagreement with the dipole selection rule.¹⁷ However, this selection rule is only valid for ideal metallic surfaces, and an experimental test of our assignment, precisely taking advantage of the surface-parallel orientation of this phonon,

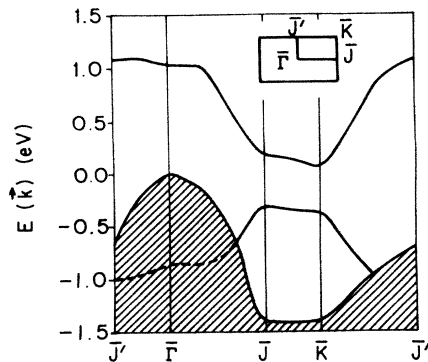


FIG. 2. Dispersion of electronic surface states and resonances for the π -bonded chain model of Si(111) 2×1 along symmetry directions on the surface Brillouin zone (inset). The hatched area represents the projected bulk states. $\bar{\Gamma} \rightarrow \bar{J}$ is parallel to the chain direction, and $\bar{J} \rightarrow \bar{K}$ is perpendicular.

has been recently done in angle-dependent EELS experiments.¹⁴ A second rather surprising result where electron-phonon coupling also plays an important role is found in the acoustic part of the phonon spectrum. Here we find a nearly dispersionless Rayleigh mode with frequency well below the bulk acoustic continuum, which is surprising given that the bonding along the surface chains is very strong. This feature in our calculated phonon spectrum is consistent with recent measurements of dispersion curves of surface phonons using He-atom scattering by Harten, Toennies, and Wöll (HTW).¹⁸ We understand this feature as a result of a strong phonon-energy renormalization effect due to virtual electronic transitions from the backbond states to the empty surface states, a subsurface mediated effect.

These two features just mentioned demonstrate how the lattice dynamics of the Si(111) 2×1 surface is different from the bulk, and the importance of explicitly incorporating the electronic degrees of freedom in any description of the vibrational properties of semiconductor surfaces. The theory we have developed to study vibrational excitations on Si surfaces is based on Chadi's¹⁹ empirical tight-binding theory for structural energies in semiconductors. In this theory the total energy of the system is expressed in terms of the electron band-structure energy, which is calculated using a tight-binding (TB) representation of the valence electrons, and a short-range elastic energy which represents the ion-ion interactions and corrects for the double counting of electron-electron interactions in the band-structure energy, that is, this term represents the screened ion-ion interactions. To this basic model we have added an on-site electron-repulsion term in the form of a Hubbard-like Hamiltonian. This represents an important improvement in the theory, since non-negligible charge transfers occur at surfaces. In addition to making geometries with large charge transfers energetically unfavorable, this repulsion term enters into the dynamical matrix by screening charge fluctuations. For the TB Hamiltonian we use an sp^3 orbital representation with electronic hopping amplitudes that scale as d^{-2} with interatomic distance d , and couple first nearest neighbors only. For the ion-ion elastic potential we also use a nearest-neighbor interaction. This empirical theory provides us with a simple, yet realistic description of structural energies for Si; it allows us to calculate phonon dispersion relations and the linear response of the system under structural perturbations, while at the same time it incorporates the electrons into the model and remains computationally tractable. A similar approach to ours has been used by Varma and Weber to study phonon anomalies in transition metals,^{20,21} and by Lee and Joannopoulos to study defects in SiC.²²

The structure of the rest of the paper is as follows. In the next section we outline the theory and the formalism to calculate phonons and dynamic charges; a detailed exposition has been presented elsewhere.²³ In Sec. III we discuss the equilibrium properties of the π -bonded chain model of the Si(111) 2×1 surface. The dispersion of the calculated surface phonons is presented in Sec. IV, and their dipole activity, or the one-phonon absorption spec-

trum of the surface, is discussed in Sec. V. We will compare our results with those of the EELS experiments of Ibach, and with the dispersion curves measured by HTW; these are the only two existing experiments on the vibrational spectroscopy of clean semiconductor surfaces (Ibach's results have been repeated by other groups^{14,24}). In Sec. VI we summarize our results. Finally, in an appendix, we briefly consider the π -bonded molecular model, proposed by Chadi²⁵ as an alternative model for the reconstruction of the surface. Here we are particularly interested in comparing the phonon excitation spectra of the chain and molecular models, and on whether the molecular model can explain the strong dipole-active surface phonon. We find that the answer to this question is no, only the chain model is consistent with the observed dipole-active surface phonon.

II. THEORY

The general program that we follow consists of three steps. (1) First, we construct an expression for the total energy of the system and find the minimum-energy configuration, or equilibrium structure. (2) Next, we take the second derivatives of the total energy to calculate the dynamical matrix, which we diagonalize to obtain the normal modes of vibration. (3) Finally, we use linear response to calculate the charge fluctuations induced by vibrational excitations, or dynamic charges; these are then used to obtain the phonon-assisted contribution to the surface conductivity. The formalism for each one of these steps is outlined in the following subsections; a detailed exposition appears in Ref. 23.

A. Total energy

We define the following Hamiltonian to describe the electron-ion system of a Si structure:

$$H = \sum_i \sum_{\lambda=s,p} \epsilon_\lambda a_{i\lambda}^\dagger a_{i\lambda} + \sum_{\langle i,j \rangle} \sum_{\lambda,\lambda'=s,p} h_{i\lambda,j\lambda'} a_{i\lambda}^\dagger a_{j\lambda'} + H_U + V, \quad (1)$$

where the first two terms are a TB representation of the valence electrons, H_U is an on-site electron repulsion term, and V is an elastic potential between the ions. In the TB Hamiltonian i labels ions, the sum $\langle i,j \rangle$ is over nearest-neighbor ions, and λ, λ' denote the TB orbitals. We use a set of sp^3 TB parameters obtained by fitting the electron bands of Si in the diamond structure;²⁶ these are listed in Table I. We let the electron-hopping ampli-

tudes $h_{i\lambda,j\lambda'}$ scale with interatomic distance following the commonly used d^{-2} rule:²⁷

$$h_{i\lambda,j\lambda'}(d) = h_{i\lambda,j\lambda'}(d_0)(d_0/d)^2.$$

Since the hybridization of the sp^3 orbitals determines the directional character of covalent bonding, in our theory the bond-bending forces are generated by the electron band structure. The second term in Eq. (1) is an on-site electron-repulsion term in the form of a Hubbard interaction:

$$H_U = \frac{1}{2} U \sum_i (\hat{n}_i - n_i^0)^2, \quad (2)$$

where the sum is over atomic sites and \hat{n}_i is the number operator:

$$\hat{n}_i = \sum_{\lambda=s,p} a_{i\lambda}^\dagger a_{i\lambda}. \quad (3)$$

The ground-state expectation value of the number operator $\langle \hat{n}_i \rangle$ gives the total valence charge at the atom i ; $\langle \hat{n}_i^0 \rangle = 4$ for the sp^3 orbital basis we are using. H_U makes geometries with large charge transfers energetically unfavorable, and represents an important improvement in the original theory, since charge transfers play an important role in reconstructed surfaces. The repulsion constant U is fixed by a surface property: we fit the minimum direct gap of the electronic surface states, giving $U = 4$ eV. Finally, we use an elastic nearest-neighbor central potential to model the screened^{19,20} ion-ion potential V :

$$V = \sum_{\langle i,j \rangle} V_1 x_{ij} + V_2 x_{ij}^2, \quad (4)$$

where $x_{ij} = d_{ij}/d_0 - 1$, and d_{ij} and d_0 are, respectively, the bond length between the ions i, j and the equilibrium value of the bond length in crystalline bulk. The elastic constants are determined by crystalline bulk properties: V_1 is chosen such that the linear term in the elastic potential plus the band-structure energy equilibrate the crystal at the experimental bond length ($d_0 = 2.35$ Å), and V_2 is a free parameter that we use to fit the optical phonon at Γ . These constants are also listed in Table I.

The expression for the total energy that we use as a starting point in the formulation of dynamical properties is written in terms of the electron band-structure energy E_{BS} :

$$E_{BS} = 2 \sum_{n\mathbf{k}} f_n(\mathbf{k}) E_n(\mathbf{k}), \quad (5)$$

where $E_n(\mathbf{k})$ are single-particle electron energies, and $f_n(\mathbf{k})$ are Fermi factors; the electron energies are solutions to the one-electron equations

$$H_{el} | \psi_n(\mathbf{k}) \rangle = E_n(\mathbf{k}) | \psi_n(\mathbf{k}) \rangle, \quad (6)$$

where H_{el} is the Hartree Hamiltonian derived from Eq. (1):

$$H_{el} = \sum_i \sum_{\lambda=s,p} [\epsilon_\lambda + U(\hat{n}_i - n_i^0)] a_{i\lambda}^\dagger a_{i\lambda} + \sum_{\langle i,j \rangle} \sum_{\lambda,\lambda'=s,p} h_{i\lambda,j\lambda'} a_{i\lambda}^\dagger a_{j\lambda'}. \quad (7)$$

TABLE I. Electronic sp^3 tight-binding parameters and elastic Hamiltonian parameters for Si.

$\epsilon_p - \epsilon_s$	6.45 eV	V_1	-16.31 eV
$h_{ss\sigma}$	-1.94 eV	V_2	49.26 eV
$h_{sp\sigma}$	1.75 eV		
$h_{pp\sigma}$	-1.08 eV		
$h_{pp\pi}$	3.05 eV		

We treat the quadratic terms in the particle operators in the mean-field approximation by replacing $\hat{n}_i a_{i\lambda}^\dagger a_{i\lambda}$ by $\langle \hat{n}_i \rangle a_{i\lambda}^\dagger a_{i\lambda}$; thus if we define U_i as the mean-field on-site interaction

$$U_i \equiv U(\langle \hat{n}_i \rangle - n_i^0), \quad (8)$$

then the one-electron Hamiltonian which enters in Eq. (5) can be written as

$$H_{el} = \sum_i \sum_{\lambda=s,p} (\varepsilon_\lambda + U_i) a_{i\lambda}^\dagger a_{i\lambda} + \sum_{\langle i,j \rangle} \sum_{\lambda,\lambda'=s,p} h_{i\lambda,j\lambda'} a_{i\lambda}^\dagger a_{j\lambda'}. \quad (9)$$

The presence of U_i in Eq. (9) implies that the one-particle equations have to be solved self-consistently. The total energy of the system is then

$$E_{tot} = E_{BS} - \sum_i \frac{1}{2} U(\langle \hat{n}_i \rangle - n_i^0)^2 + V. \quad (10)$$

E_{tot} depends explicitly and implicitly on the ionic coordinates. Starting at some given initial ionic configuration, with the connectivity of the system defined as an input into the problem, we find the equilibrium configuration by following the forces on the system, which we calculate using the Hellmann-Feynman theorem:

$$F_\alpha = - \left\langle \frac{\partial H_{el}}{\partial x_\alpha} \right\rangle + \left\langle \frac{\partial H_U}{\partial x_\alpha} \right\rangle - \frac{\partial V}{\partial x_\alpha},$$

$$\begin{aligned} \frac{\partial^2 \langle H_{el} \rangle}{\partial x_\alpha^* (\mathbf{q}) \partial x_\beta (\mathbf{q})} &= 2 \sum_{n,\mathbf{k}} f_n(\mathbf{k}) \left\langle \psi_n(\mathbf{k}) \left| \frac{\partial^2 H_{el}}{\partial x_\alpha^* (\mathbf{q}) \partial x_\beta (\mathbf{q})} \right| \psi_n(\mathbf{k}) \right\rangle \\ &+ 2 \sum_{n,\mathbf{k}} \sum_{n',\mathbf{k}'} \frac{f_n(\mathbf{k}) - f_{n'}(\mathbf{k}')}{E_n(\mathbf{k}) - E_{n'}(\mathbf{k}')} \left\langle \psi_n(\mathbf{k}) \left| \frac{\partial H_{el}}{\partial x_\alpha^* (\mathbf{q})} \right| \psi_{n'}(\mathbf{k}') \right\rangle \left\langle \psi_{n'}(\mathbf{k}') \left| \frac{\partial H_{el}}{\partial x_\beta (\mathbf{q})} \right| \psi_n(\mathbf{k}) \right\rangle. \end{aligned} \quad (12)$$

The last term in Eq. (11), the elastic contribution to $D_{\alpha\beta}(\mathbf{q})$, is straightforward to calculate

$$V_{ii'} = V_1 \left[\frac{r_{ii'}}{d_0} - 1 \right] + V_2 \left[\frac{r_{ii'}}{d_0} - 1 \right]^2, \quad (13a)$$

$$\frac{\partial^2 V_{ii'}}{\partial x_{i\mu} \partial x_{j\nu}} = \frac{(\delta_{ij} - \delta_{i'j'})}{r_{ii'} d_0} \left\{ [\delta_{\mu\nu} - (\hat{r}_{ii'}^\mu (\hat{r}_{ii'}^\nu))] \left[V_1 + V_2 \left[\frac{r_{ii'}}{d_0} - 1 \right] \right] - (\hat{r}_{ii'}^\mu (\hat{r}_{ii'}^\nu) 2V_2 \right\}. \quad (13b)$$

Here $\alpha = (i, \mu)$ and $\beta = (j, \nu)$ where μ, ν label Cartesian coordinates. Both the first term in Eq. (12) and that in Eq. (13) contain only short-range forces (the electronic hopping amplitudes and the elastic potential couple only nearest neighbors). On the other hand, the second term in Eq. (12), which represents the electron polarization, does generate long-range forces; it introduces lattice interactions that are mediated by the exchange of electron-hole pairs. If we denote the electron-phonon matrix elements by $g_{n'\mathbf{k}',n\mathbf{k}}^\alpha(\mathbf{q})$:

$$g_{n'\mathbf{k}',n\mathbf{k}}^\alpha(\mathbf{q}) = \left\langle \psi_{n'}(\mathbf{k}') \left| \frac{\partial H_{el}}{\partial x_\alpha (\mathbf{q})} \right| \psi_n(\mathbf{k}) \right\rangle, \quad (14)$$

where x_α is an ionic coordinate. The second term in the above equation is zero, since the number operator does not depend explicitly on $\{x_\alpha\}$. We use a conjugate gradient algorithm for the global search of the absolute minimum of energy, and a more direct Newton's method once the search is close to that minimum.

B. Phonons

Once the equilibrium configuration has been found we proceed to calculate the dynamical matrix, given by the second derivatives of the ground-state energy with respect to the structural degrees of freedom:

$$D_{\alpha\beta}(\mathbf{q}) = \frac{\partial^2 \langle H_{el} \rangle}{\partial x_\alpha^* (\mathbf{q}) \partial x_\beta (\mathbf{q})} - \frac{\partial^2 \langle H_U \rangle}{\partial x_\alpha^* (\mathbf{q}) \partial x_\beta (\mathbf{q})} + \frac{\partial^2 V}{\partial x_\alpha^* (\mathbf{q}) \partial x_\beta (\mathbf{q})}. \quad (11)$$

The derivatives are taken with respect to spatially modulated displacements with wave vector \mathbf{q} (this can be done since the structures we are studying are periodic, and the interactions in the model have finite range). We will reserve \mathbf{k} for the electron energies and eigenstates and \mathbf{q} for the phonons. The first term in Eq. (11) leads to two terms, the first one being quadratic in the electron-phonon coupling and the second one linear in the electron-phonon coupling taken to second order in perturbation theory:

then the electron polarization contribution to $D_{\alpha\beta}(\mathbf{q})$ can be written as

$$D_{\alpha\beta}^{pol}(\mathbf{q}) = 2 \sum_{n,\mathbf{k}} \sum_{n',\mathbf{k}'} \frac{f_n(\mathbf{k}) - f_{n'}(\mathbf{k}')}{E_n(\mathbf{k}) - E_{n'}(\mathbf{k}')} g_{n\mathbf{k},n'\mathbf{k}'}^\alpha(-\mathbf{q}) \times g_{n'\mathbf{k}',n\mathbf{k}}^\beta(\mathbf{q}). \quad (15)$$

Finally, the repulsion H_U enters into the expression for $D_{\alpha\beta}(\mathbf{q})$ by dynamically screening the charge fluctuations in $D_{\alpha\beta}^{pol}(\mathbf{q})$. Note that the self-consistent electron states that enter into the polarization sum are already statically

screened. The dynamic screening has the form²³

$$D_{\alpha\beta}^U(\mathbf{q}) = U \delta n_{\alpha}^{(0)\dagger}(\mathbf{q}) [\mathbf{I} - U\chi(\mathbf{q})]^{-1} \delta n_{\beta}^{(0)}(\mathbf{q}), \quad (16)$$

where χ is the density-density correlation function

$$\begin{aligned} \chi_{i,j}(\mathbf{q}) = & 2 \sum_{n,\mathbf{k}} \sum_{n',\mathbf{k}'} \frac{f_n(\mathbf{k}) - f_{n'}(\mathbf{k}')}{E_n(\mathbf{k}) - E_{n'}(\mathbf{k}')} \\ & \times \langle \psi_n(\mathbf{k}) | \hat{n}_i(-\mathbf{q}) | \psi_{n'}(\mathbf{k}') \rangle \\ & \times \langle \psi_{n'}(\mathbf{k}') | \hat{n}_j(\mathbf{q}) | \psi_n(\mathbf{k}) \rangle, \quad (17) \end{aligned}$$

and $\delta n_{\beta}^{(0)i}$ are the linearized density fluctuations in response to the lattice fluctuation x_{β} :

$$\begin{aligned} \delta n_{\beta}^{(0)i}(\mathbf{q}) = & 2 \sum_{n,\mathbf{k}} \sum_{n',\mathbf{k}'} \frac{f_n(\mathbf{k}) - f_{n'}(\mathbf{k}')}{E_n(\mathbf{k}) - E_{n'}(\mathbf{k}')} \\ & \times \langle \psi_n(\mathbf{k}) | \hat{n}_i(\mathbf{q}) | \psi_{n'}(\mathbf{k}') \rangle \\ & \times \left\langle \psi_{n'}(\mathbf{k}') \left| \frac{\partial H}{\partial x_{\beta}(\mathbf{q})} \right| \psi_n(\mathbf{k}) \right\rangle. \quad (18) \end{aligned}$$

All these terms can be combined to express $D_{\alpha\beta}(\mathbf{q})$ in the following form:

$$\begin{aligned} \langle \mathbf{J}(t) \rangle_{\alpha} = & 2 \sum_{n,n'} \sum_{\mathbf{k}} [f_n(\mathbf{k}) - f_{n'}(\mathbf{k})] \left[\frac{2 \cos(\omega t)}{E_n(\mathbf{k}) - E_{n'}(\mathbf{k})} [\mathbf{J}(n\mathbf{k}, n'\mathbf{k}) h_{\alpha}(n'\mathbf{k}, n\mathbf{k}) + \mathbf{J}(n'\mathbf{k}, n\mathbf{k}) h_{\alpha}(n\mathbf{k}, n'\mathbf{k})] \right. \\ & \left. + \frac{2i\omega \sin(\omega t)}{[E_n(\mathbf{k}) - E_{n'}(\mathbf{k})]^2} [\mathbf{J}(n\mathbf{k}, n'\mathbf{k}) h_{\alpha}(n'\mathbf{k}, n\mathbf{k}) - \mathbf{J}(n'\mathbf{k}, n\mathbf{k}) h_{\alpha}(n\mathbf{k}, n'\mathbf{k})] \right], \quad (21) \end{aligned}$$

where $\mathbf{J}(n\mathbf{k}, n'\mathbf{k})$ and $h_{\alpha}(n\mathbf{k}, n'\mathbf{k})$ are the matrix elements of the current density operator and the perturbation h_{α} :

$$\begin{aligned} \mathbf{J}(n\mathbf{k}, n'\mathbf{k}) &= \langle \psi_n(\mathbf{k}) | \mathbf{J} | \psi_{n'}(\mathbf{k}') \rangle, \\ h_{\alpha}(n\mathbf{k}, n'\mathbf{k}) &= \langle \psi_n(\mathbf{k}) | h_{\alpha} | \psi_{n'}(\mathbf{k}') \rangle. \quad (22) \end{aligned}$$

The dynamic charges $\{e_{\alpha}^*\}$ are defined by writing the oscillating current density in terms of a dipole moment:

$$\langle \mathbf{J}(t) \rangle_{\alpha} = e_{\alpha}^* \dot{x}_{\alpha}(t) = e_{\alpha}^* \dot{x}_{\alpha}^0 i \omega (e^{i\omega t} - e^{-i\omega t}). \quad (23)$$

Combining this definition and Eq. (22), we obtain an expression for e_{α}^* :

$$\begin{aligned} e_{\alpha}^* = & 2 \sum_{n,n'} \sum_{\mathbf{k}} i \frac{f_n(\mathbf{k}) - f_{n'}(\mathbf{k}')}{[E_n(\mathbf{k}) - E_{n'}(\mathbf{k}')]^2} \\ & \times [\mathbf{J}(n\mathbf{k}, n'\mathbf{k}) h_{\alpha}(n'\mathbf{k}, n\mathbf{k}) \\ & - \mathbf{J}(n'\mathbf{k}, n\mathbf{k}) h_{\alpha}(n\mathbf{k}, n'\mathbf{k})]. \quad (24) \end{aligned}$$

In order to evaluate Eq. (24) we use the following identity for the current density operator:

$$D_{\alpha\beta}(\mathbf{q}) = D_{\alpha\beta}^{\text{SR}}(\mathbf{q}) + D_{\alpha\beta}^{\text{pol}}(\mathbf{q}) + D_{\alpha\beta}^U(\mathbf{q}), \quad (19)$$

where the short-range terms are combined in $D_{\alpha\beta}^{\text{SR}}(\mathbf{q})$, and the last two terms, which represent the screened electron polarizability, generate the long-range forces in our theory. The eigenvalues of $D_{\alpha\beta}(\mathbf{q})$ are $M\omega_n^2(\mathbf{q})$, where $\hbar\omega_n(\mathbf{q})$ is the energy of the n th normal mode of vibration and $Q_{\alpha}^{(n)}$ is its displacement field.

C. Dynamic charges

The vibrations of the lattice can generate fluctuations of the electron charge density; these vibrationally excited charge fluctuations are parametrized by the dynamic charges of the system. We obtain dynamic charges in our theory by calculating the linearized dynamic response of the current density to a perturbation generated by a lattice fluctuation. This perturbation is

$$H^1(t) = h_{\alpha} (e^{i\omega t} + e^{-i\omega t}), \quad (20)$$

where $h_{\alpha} = (\partial H / \partial x_{\alpha}) \delta x_{\alpha}$, and ω is a phonon frequency. We are interested in the phonon dipole activity, so that only optical transitions have to be considered and therefore the lattice perturbation h_{α} has no spatial modulation ($\mathbf{q}=0$). The linearized response of the current density to this perturbation is²³

$$\mathbf{J} = -\frac{ie}{\hbar} [\mathbf{r}, H]. \quad (25)$$

Notice that the first term in Eq. (21), which is in phase with the perturbing potential and out of phase with $\dot{x}_{\alpha}(t)$, does not contribute to e_{α}^* as written in Eq. (24). Indeed the Brillouin-zone integration in Eq. (21), with time reversal, yields this result. As long as the driving frequency is slower than the fastest response of the system, as it is since $\omega < E_G$, this result ought to hold. However, if higher-order terms in the $\omega/[E_n(\mathbf{k}) - E_{n'}(\mathbf{k}')]^2$ expansion of the time-dependent perturbation expression for $\langle \mathbf{J} \rangle$ are kept,²³ a nonvanishing in-phase contribution survives.

If the dynamic charges e_{α}^* are projected onto the normalized displacement field $Q_{\alpha}^{(n)}$ of the n th phonon of the system, we obtain the dynamic charge e_n^* associated with that particular normal mode of vibration:

$$e_n^* = \sum_{\alpha} e_{\alpha}^* Q_{\alpha}^{(n)}. \quad (26)$$

The phonon-assisted contribution to the surface conductivity then follows:

$$\sigma_1^\mu(\omega) = \frac{\pi}{2MA} \sum_n |(\mathbf{e}_n^*)_\mu|^2 [\delta(\omega - \omega_n) + \delta(\omega + \omega_n)], \quad (27)$$

where the sum is over the $\mathbf{q}=0$ phonon modes, M is the ionic mass (28 amu for Si), and A is the area of the surface unit cell. The subscript 1 denotes, as usual, the real part, and the superscript μ denotes Cartesian coordinate. $\sigma_1(\omega)$ is the infrared (ir) one-phonon absorption spectrum of the surface, or phonon dipole activity. The absolute one-phonon ir absorption coefficient $\alpha(\omega)$ is related to $\sigma_1(\omega)$ by the following expression:²⁸

$$\alpha(\omega) = \frac{4\pi\sigma_1(\omega)}{nc}, \quad (28)$$

where n is the electronic ir index of refraction and c is the speed of light.

D. Technical considerations

We represent the surface with a slab geometry, with two identical surfaces on each side. We use a 14-layer slab which has an inversion symmetry point at its center; this slab is thick enough so that its middle part is a good representation of the bulk and the two opposite surfaces are nearly decoupled: electronic surface states localized on each one of the two surfaces are nearly degenerate, and surface-phonon splitting is no larger than 1–2 meV for surface-localized modes. Still, some effects due to the finite slab thickness appear in the long-wavelength part of the phonon spectrum, as we will discuss later; this is not surprising since in this limit the slab is essentially a thin film.

The surface Brillouin zone (SBZ) for Si(111) 2×1 is shown in the inset in Fig. 2. The irreducible zone is the area enclosed by $\bar{\Gamma}-\bar{J}-\bar{K}-\bar{J}'$, it is defined by time reversal and by a mirror-plane symmetry that is normal to the chain direction $\bar{\Gamma}-\bar{J}$. This is the only symmetry of the surface (C_v symmetry group). The electron equations (6) are solved on a grid of 16 k points in the irreducible zone. The dynamical matrix is explicitly calculated for the set of \mathbf{q} points that connect two k points

(the electron-phonon matrix elements impose the constraint $\mathbf{k}' = \mathbf{k} + \mathbf{q}$); we can then obtain the dynamical matrix for any arbitrary wave vector by Fourier transforming the set of dynamical matrices on the original \mathbf{q} -point grid into a set of real-space force constants, and then we backtransform to \mathbf{q} space. In doing this the approximation is made that force constants beyond the size of the Born–von Kármán supercell defined by the original k -point grid are taken as zero; in our calculations we include force constants up to the sixth-nearest-neighbor unit cell, corresponding to ions separated by as much as 25 Å. We only explicitly calculate the dynamical matrix, as outlined in Sec. II B, for \mathbf{q} points inside the irreducible zone; for \mathbf{q} outside this zone we use time-reversal

$$D_{i\mu,j\nu}(-\mathbf{q}) = D_{i\mu,j\nu}^*(\mathbf{q}), \quad (29)$$

and the mirror-plane symmetry σ

$$D_{i\mu,j\nu}(\sigma\mathbf{q}) = e^{i(\mathbf{q}-\sigma\mathbf{q}) \cdot (\tau_j - \tau_i)} \sum_{\gamma,\delta} \sigma_{\mu\gamma} \sigma_{\nu\delta} D_{i\gamma,j\delta}(\mathbf{q}), \quad (30)$$

where i, j denote atoms in the unit cell, τ_i is a basis vector, and greek letters denote Cartesian coordinates.

III. THE π -BONDED CHAIN MODEL, EQUILIBRIUM STRUCTURE

The coordinates of the equilibrium configuration of the surface that we obtain in our calculations are listed in Table II; our results compare well with LEED (Ref. 8) and ion-scattering experiments,²⁹ but we overestimate the tilt of the chains. The bond length along the surface chains remains essentially unchanged with respect to the bulk bond length. In Fig. 2 we show the calculated electronic surface bands. There are two surface bands, since there are two surface electrons per unit cell; one is filled and the other one is empty. Close to the zone center the filled band is actually a surface resonance. Both the filled and the empty surface bands have strong dispersion along $\bar{\Gamma}-\bar{J}$ (parallel to the chain direction), and very weak dispersion along $\bar{J}-\bar{K}$ (perpendicular to the chains). That is, the dispersion of the surface electrons along the chains follows nearly-free-electron behavior,

TABLE II. Equilibrium coordinates of the π -bonded chain model of the reconstruction of the Si(111) 2×1 surface. The atom numbering corresponds to Fig. 1(d) and the origin is chosen at the center of the slab on atom 13. Coordinates given in units of $d_0 = 2.35$ Å, the bond length of diamond-structure silicon. Cartesian coordinates are assigned as follows: $x \rightarrow \langle 1\bar{1}0 \rangle$, $y \rightarrow \langle 11\bar{2} \rangle$, $z \rightarrow \langle 111 \rangle$.

Atom No.	x	y	z	Atom No.	x	y	z
1	0.00	-2.43	3.98	2	0.82	-2.92	4.25
3	0.00	-1.50	3.60	4	0.82	-3.73	3.63
5	0.00	-1.86	2.66	6	0.82	-3.36	2.68
7	0.00	-0.94	2.28	8	0.82	-2.38	2.39
9	0.00	-0.94	1.30	10	0.82	-2.37	1.37
11	0.00	0.00	1.00	12	0.82	-1.43	1.00
13	0.00	0.00	0.00	14	0.82	-1.42	0.00

with a small gap at the zone edge (small compared to the bulk gap 1.17 eV), and the chains are essentially decoupled from each other. The minimum direct gap E_G occurs at \bar{K} and remains fairly constant throughout the entire zone edge $\bar{J}-\bar{K}$ (at \bar{J} the direct gap is 0.5 eV). This gap has been measured in many experiments using a variety of techniques (optical absorption and reflection, electron spectroscopy, and STM):³⁰ $E_G=0.45$ eV. The value of the repulsion constant U is chosen to reproduce the value of this gap: $U=4.0$ eV. These bands have been previously calculated using more precise first-principles theories, and the agreement with experiment is very good.^{4,3} Our calculated bands also compare well with experiment. The filled band has been traced using ultraviolet ARUPS photoemission experiments^{9,10} (ARUPS) and in angle-resolved EELS experiments,¹³ and the empty surface band has been traced using inverse ARUPS.^{11,12} Experimentally, the filled band disperses up from $\bar{\Gamma}$ to \bar{J} by 0.6–0.7 eV and down from $\bar{\Gamma}$ to \bar{J}' by 0.2–0.3 eV. In our bands these dispersions are ~ 0.65 eV up from $\bar{\Gamma}$ to \bar{J} , and ~ 0.1 down from $\bar{\Gamma}$ to \bar{J}' . In our bands there is a slight downward dispersion ~ 0.1 eV from \bar{J} to \bar{K} , but no appreciable dispersion is measured along the zone edge.

The value of the gap is very closely related to two structural degrees of freedom of the surface zigzag chains: tilt and dimerization (the chains are tilted, but not dimerized in equilibrium). We discuss each one of these separately.

Tilt. There is a nonzero gap E_G between the filled and empty surface bands because the two surface atoms on the unit cell are asymmetric: the surface atoms along a chain are inequivalent with respect to the subsurface and the zigzag chains are tilted. The value of the tilt is $\Delta z=0.6$ Å or 15° in our calculations; experimentally, it is found to be 0.38 ± 0.08 Å in LEED (Ref. 8) and 0.3 ± 0.35 Å in MEIS.³¹ This last experiment finds that the second-layer chains are also tilted by 0.1 ± 0.2 Å; we find this tilt to be 0.06 Å. According to our calculations the up atoms gain $\sim 0.13e$ and the down atoms lose $\sim 0.21e$. These small charge transfers are consistent with the small core-level shifts observed experimentally³² and with the theoretical results of Pandey³³ (gain of $\sim 0.25e$ for the up atoms and loss of $\sim 0.15e$ for the down atoms). The subsurface asymmetry is responsible for less than 0.1 eV of the total gap 0.45 eV. The further opening of the gap, which reduces the band-structure energy, drives the charge transfer. The on-site electronic repulsion H_U introduces a competing effect to this charge transfer; the larger the repulsion constant U the smaller the charge transfer and the gap E_G . The addition of H_U to the theoretical model represents an important improvement in the description of the electronic properties of the surface; with $U=0$ the electronic surface bands would be qualitatively different from Fig. 2, with a minimum direct gap of ~ 1.0 eV. H_U effectively reduces the charge transfer between the up and down atoms in the “bare” Chadi model, and we obtain surface bands that are in good agreement with experiment. However, the tilt Δz of the surface chains is unaffected by H_U , and we probably overestimate its value.

Dimerization. In the equilibrium configuration the surface chains are not dimerized. It is natural to expect, however, that this is an important degree of freedom of the surface (consider the resemblance of the surface chains to polyacetylene). Indeed, an LO vibrational mode along the chains, which dimerizes them, drives an anomalously large charge fluctuation, and as we have already mentioned, this mode dominates the phonon absorption spectrum of the surface. At equilibrium the chains are not dimerized, and the surface has a mirror-plane symmetry, where the mirror plane is normal to the chain direction $\langle 1\bar{1}0 \rangle$. A number of experiments have verified the existence of this mirror-plane symmetry.^{34–36}

IV. SURFACE PHONONS

The calculated phonon dispersion curves for the chain model of Si(111) 2×1 are shown in Fig. 3. Surface phonons are represented with solid lines and surface resonances with dashed lines. There are surface phonons outside both ends of the bulk spectrum. The one below the bottom of the acoustic continuum is the Rayleigh wave, which occurs on all surfaces, although on this surface the Rayleigh wave has quite peculiar behavior, described below. A surface phonon above the optical continuum, on the other hand, is not expected to occur on surfaces in general, and is related to the reconstructed geometry of the chain model. Both of these will be discussed later. Among the surface resonances at $\bar{\Gamma}$ we find a spectrum of modes that have the form of elementary vibrational excitations of the surface chains, including a longitudinal-optical mode along the chains, and a transverse-optical mode normal to the surface plane; these two phonons are related, respectively, to the dimerization and tilt of the chains discussed above. These and other surface modes are schematically illustrated in Fig. 4.

We divide the discussion of the phonon spectrum in

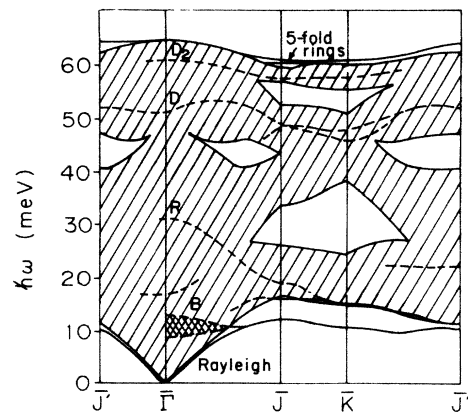


FIG. 3. Phonon dispersion curves for the π -bonded chain model of Si(111) 2×1 . Solid lines are surface phonons and dashed lines surface resonances. The hatched regions represent the projected bulk modes, and the dashed area near the zone center corresponds to a broad surface resonance.

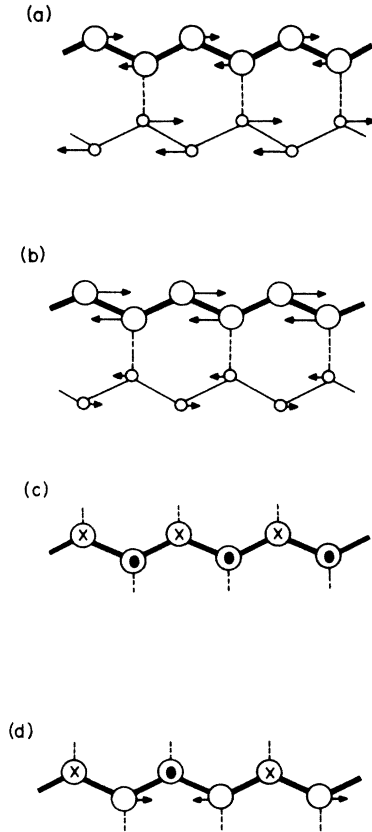


FIG. 4. Schematic representation of vibrational modes that have the form of elementary vibrational excitations of the surface chains. Zone center: (a) LO subsurface phonon along the chains (subsurface dimer mode D_2), (b) LO surface phonon along the chains (dimer mode D), (c) TO phonon normal to the surface (rocking mode R). Zone edge: (d) N_1 , lowest-lying Rayleigh mode at \bar{J} .

Fig. 3 in two parts, corresponding to the optical and acoustic regions of the projected bulk phonons. This is not a perfectly well-defined division in terms of phonon energies, but we assign the region from 40 meV upwards as the optical region, and the lower part of the spectrum as the acoustic region. Surface phonons in the acoustic region are experimentally accessible using atom scattering or infrared spectroscopy, and electron scattering (EELS) can be used to study the entire spectrum. As mentioned earlier, we will make contact with results from EELS and He-atom experiments. The energies of the most important features in the spectrum at $\bar{\Gamma}$ are listed in Table III.

A. Optical phonons

We discuss the most relevant features of the optical region of the surface phonon spectrum.

Fivefold ring mode. When a surface is created, the most important perturbation on the atoms that sit at the surface is the reduction in their coordination number. This explains why the Rayleigh wave is usually below the acoustic continuum. For the same reason, it is quite surprising to observe that the phonon spectrum of the

TABLE III. Energies (in meV) of surface phonons and resonances (R) at $\bar{\Gamma}$ for the π -bonded chain model of the Si(111) 2×1 surface. Symmetry (+, even; -, odd) is with respect to the mirror-plane symmetry normal to the chain direction $\langle 1\bar{1}0 \rangle$.

$\bar{\Gamma}$	
B , surface chain bounce (R)	10.0 +
R , rocking mode	31.0 +
D , dimer mode	51.0-
D_2 , subsurface dimer mode	61.0-

Si(111) 2×1 surface includes modes with higher frequency than the bulk vibrations. In fact, there are two surface phonons that are above the optical continuum for a considerable part of the SBZ. The explanation of this feature lies in the fivefold rings of the chain reconstruction of the surface. Roughly speaking, fivefold rings are stiffer than sixfold rings, and both of the high-frequency surface phonons are localized around the fivefold rings. In the highest one there is a large vibrational amplitude that corresponds to the stretching of the bond between atoms 3 and 5 [see Fig. 1(b)], and in the lower one the bond between atoms 4 and 6 is stretched. Both of these are back bonds that delineate the subsurface fivefold rings, and the geometry of the reconstructed surface suggests that the bond between atoms 3 and 5 is stiffer than the bond between atoms 4 and 6 (atom 3 is connected to the down atom in the surface chains, and atom 2 is connected to the up atom). Thus the two high-frequency surface phonons result from the stretching of the back bonds that participate in the subsurface fivefold rings. We briefly mention here that the reconstruction of the Si(001) surface also includes fivefold rings, and in its phonon spectrum, which we have calculated,^{37,23} high-frequency modes above the top of the optical continuum also appear. One might speculate that high-frequency phonons appear whenever fivefold rings are present, and this property could be used to identify their presence in a variety of structures, like grain boundaries and amorphous Si.

Dimer mode. Going down the energy scale in the phonon spectrum, we find a surface resonance that appears across the entire SBZ. This vibration corresponds to one of the elementary excitations of the chains: at $\bar{\Gamma}$ it has the form of a longitudinal-optical (LO) vibration along the surface chains, that is, it dimerizes the surface chains. The mirror-plane symmetry of the surface divides the zone-center modes into two categories: even and odd modes. Even modes are polarized parallel to the mirror plane (i.e., along the surface normal and perpendicular to the chain direction), and odd modes are polarized along the chain direction, parallel to the surface. The longitudinal-optical model of the chains is odd; it has vibrational amplitude only parallel to the chain direction. Because of this, it is not only a resonance at $\bar{\Gamma}$, but a proper surface phonon: even though it does not lie in an energy gap it is in a symmetry gap. This model is transverse with respect to the $\langle 111 \rangle$ direction and it is in the region of projected bulk modes that

are longitudinal with respect to $\langle 111 \rangle$. Outside $\bar{\Gamma}$ it is a very sharp resonance. The longitudinal-optical phonon of the surface chains is the surface phonon that we assign as the anomalously strongly dipole-active surface phonon seen on the Si(111) 2×1 surface. This is discussed in Sec. V.

Subsurface dimer mode. There are actually two versions of the LO mode of the surface chains, and this is related to the atoms in the second layer below the surface which also form zigzag chains, parallel to the surface chains (see Fig. 1). The first of them, the dimer mode discussed above, corresponds to a vibration where the surface and subsurface chains are moving in phase, and most of the vibrational amplitude is on the surface chains (the ratio of vibrational amplitude between the surface atoms and the subsurface atoms is 5/1). In the second version the surface and subsurface chains move out of phase, and most of the vibrational amplitude is on the subsurface chains (with ratio 1/4). We will refer to the first one as the "dimer" or LO mode of the surface chains, and to the second one as the subsurface dimer mode. They are labeled D and D_2 , respectively, in Fig. 3. Their energies at the zone center are 51 meV for the surface dimer mode and 61 meV for the subsurface dimer mode.

B. Acoustic phonons

A closeup of the acoustic region of the surface-phonon spectrum of Fig. 3 is shown in Fig. 5. In the long-wavelength limit, near $\bar{\Gamma}$, there are three phonon branches. One is the Rayleigh wave, which appears on all surfaces and corresponds to the elastic vibration of a semi-infinite system. The vibrational amplitude of the Rayleigh wave decays exponentially into the bulk and has linear dispersion near $\bar{\Gamma}$. In our calculated spectrum, however, the Rayleigh wave has q^2 dispersion instead. This difference arises because of the slab geometry we use: at long wavelengths the slab vibrates like a thin film. The other two branches correspond to the transverse-optical (TO) and transverse-acoustic (TA)

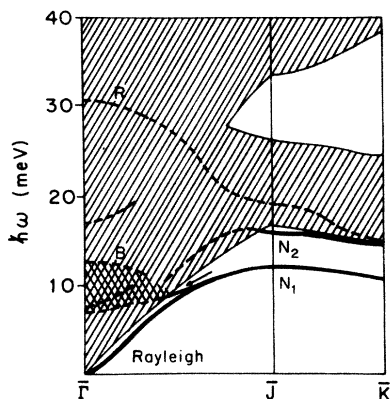


FIG. 5. Acoustic region of the phonon spectrum in Fig. 3. R , rocking mode. B , bouncing mode; N_1 , vibration normal to the surface plane of the up-atom sublattice; N_2 , analogous vibration for the down-atom sublattice.

vibrations of the surface zigzag chains, where the surface atoms oscillate along the surface normal. The TA branch, with energy 31 meV at $\bar{\Gamma}$, has the form of a rocking vibration of the chains, where the surface atoms move out of phase; it is labeled R in Fig. 5 and is schematically shown in Fig. 4(c). The TA branch appears as a broad resonance centered about 10 meV and is labeled B in Fig. 5; it corresponds at $\bar{\Gamma}$ to a bouncing vibration of the chains, where an entire surface chain moves in phase with respect to the subsurface.

Consider for the moment the surface zigzag chains as a polymer made up of two unequal atoms absorbed on the subsurface (not only the structure of the surface chains, but also the electronic surface bands are similar to those of polyacetylene). Within this picture the rocking and bouncing phonons of the surface correspond to the torsional or transverse vibrations of the polymer. In a free polymer the TA mode at the zone center has zero energy, on the surface it has finite energy at $\bar{\Gamma}$ since the surface chains are bonded to the subsurface. Again for a free polymer, the TA phonon disperses upwards from the zone center to the zone edge, and the TO phonon disperses downwards. At the zone boundary the two branches are separated by a gap due to the mass difference or inequivalence of the two types of atoms that make up the polymer; the vibrational amplitude of the mode above the gap is on the sublattice of the light atoms, and for the mode below the gap the vibrational amplitude is on the sublattice of heavy atoms. We go back now to the Si(111) 2×1 surface. At the zone center the bouncing and rocking modes correspond, respectively, to the TA and TO vibrations of the free polymer, and at the zone edge the surface phonons labeled N_1 and N_2 correspond to the polymer zone boundary modes: for N_1 the vibrational amplitude is mostly on the up atoms of the surface chains, and for N_2 it is mostly on the down surface atoms [see Fig. 4(d)]. Now we discuss the dispersion of these phonons. Given that the surface zigzag chains are strongly bonded one would expect the chain TA and TO phonons to show strong dispersion from $\bar{\Gamma}$ to the zone edge, similar to the dispersion of the electron surface bands. The rocking or TO branch does indeed follow this: it is strongly dispersive from $\bar{\Gamma}$ to \bar{J} , and has much weaker dispersion along the zone edge; it remains a resonance throughout the SBZ. The behavior of the bouncing or TA phonon, however, is very different; it remains a broad resonance with no dispersion until it reaches the edge of the bulk continuum. At this point this resonance and the Rayleigh wave seem to undergo mode repulsion (which is allowed by symmetry, since both vibrations are normal to the surface), avoiding a true crossing. This mode repulsion cannot be seen clearly because of the broadening of the resonance. Of the two branches that emerge, N_2 continues with typical Rayleigh-wave dispersion, though as a resonance inside the bulk continuum;³⁸ it eventually becomes a surface phonon at the zone edge, just off the acoustic continuum. The second branch N_1 continues as a very weakly dispersive surface phonon across the SBZ (note the energy scale in the figure). Considering the strong bonding of the surface chains, as evidenced by the

strong dispersion of the TO branch and the surface-electron bands, this is a rather surprising result. (The mode that merges with the Rayleigh wave just outside the bulk continuum, marked with an arrow in Fig. 5, is an artifact of the slab geometry that we use. N_1 is two-fold degenerate in a slab with a surface-localized mode on each one of its two identical surfaces; the mode that merges with the Rayleigh wave indicated with the arrow is a “breathing” vibration of the slab, and it would not appear in a semi-infinite system.)

This unexpected weakly dispersive acoustic surface phonon has been observed experimentally. Using inelastic He-atom scattering, HTW measured dispersion curves of surface phonons in the acoustic part of the spectrum. Besides the usual Rayleigh wave, they found a low-energy (10.5 meV), nearly dispersionless surface phonon across the SBZ. This led to the speculation¹⁸ that the observed dispersionless surface phonon is an Einstein mode, corresponding to the vibration of independent localized oscillators. The chain model cannot support such a surface phonon, thus this interpretation of the experiment implies that one ought to consider alternative models for the reconstruction of Si(111) 2×1 , and it was suggested that Chadi’s π -bonded molecular model²⁵ might explain this result. However, our results show that the chain model is indeed consistent with the appearance of a weakly dispersive, low-energy acoustic surface phonon, and that this surface phonon is not an Einstein mode. Its vibrational character depends on the wave vector; at $\bar{\Gamma}$ it is the bouncing mode of the chains, and at the zone edge it is localized on the up-atom sublattice of the chains. We will argue next that a strong phonon-energy renormalization effect causes the otherwise dispersive surface branch $B \rightarrow N_1$ to appear as weakly dispersive. As we mentioned in the Introduction, this phonon-softening effect is generated by virtual transitions from the back-bond states at the zone center to the zone-edge empty surface states, a subsurface-mediated mechanism.

At the heart of our analysis is the effect of the electrons on the surface lattice dynamics. Besides the small direct gap between the electronic surface states at the SBZ edge, there is another small gap in these bands, an indirect gap between the zone-center back-bond states, or valence-band states, and the empty surface-state states along the zone edge $\bar{J}-\bar{K}$. It might be expected then that the polarization of these electrons, through $D_{\alpha\beta}^{\text{pol}}(\mathbf{q})$ [Eq. (15)], can cause a significant softening effect for vibrations with wave vector $\mathbf{q}=\bar{J}$ (and along the entire line $\bar{J}-\bar{K}$). In order to investigate this question, we have broken the dynamical matrix in two parts: the contribution to $D_{\alpha\beta}^{\text{pol}}(\mathbf{q})$ from the electronic excitations from the valence-band states to the empty surface states, and all the rest of the dynamical matrix (including the remaining electronic transitions and the short-range interactions). We denote the corresponding phonon frequencies $\omega_{\text{VB} \rightarrow \text{SS}}$ and ω_{elastic} , respectively. Of course $\omega_{\text{tot}}^2 = \omega_{\text{VB} \rightarrow \text{SS}}^2 + \omega_{\text{elastic}}^2$. In Fig. 6 these three energies for the weakly dispersive mode ($B \rightarrow N_1$) are plotted as a function of wave vector along the chain direction on the SBZ. In the region where this branch broadens, and

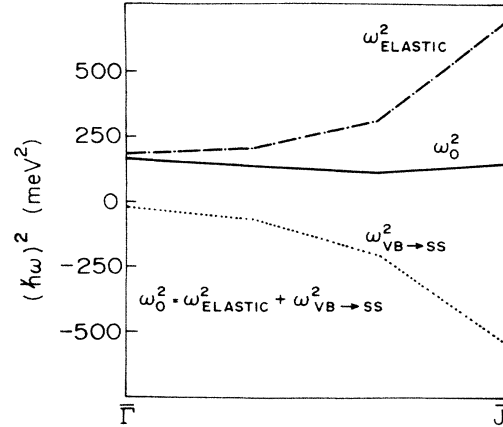


FIG. 6. Dispersion of ω_{tot}^2 , $\omega_{\text{elastic}}^2$, and $\omega_{\text{VB} \rightarrow \text{SS}}^2$ along the chain direction on the SBZ.

where the modes seem to cross, we calculate an average in order to clarify the figure and our discussion. Contrary to the nearly dispersionless character of ω_{tot}^2 , both $\omega_{\text{VB} \rightarrow \text{SS}}^2$ and $\omega_{\text{elastic}}^2$ separately show rather strong dispersion. Actually, $\omega_{\text{elastic}}^2$ has the behavior expected from the surface chains, but its upward dispersion is almost completely canceled by the sharp softening in $\omega_{\text{VB} \rightarrow \text{SS}}^2$ at the zone edge. Notice that due to the strong dispersion of the surface electron bands the small indirect gap occurs only for $\mathbf{q}=\bar{J}$; therefore, the softening effect of $D_{\alpha\beta}^{\text{pol}}(\mathbf{q})$ is sharply enhanced only close to \bar{J} . Were the surface electron bands weakly dispersive, $\omega_{\text{VB} \rightarrow \text{SS}}^2$ would be fairly constant throughout the SBZ and ω_{tot}^2 would follow the upward dispersion of $\omega_{\text{elastic}}^2$. Our calculation shows that the electron-phonon matrix elements for the in-phase vibration of the surface chains, the bouncing mode, have a large modulation effect on the surface-terminated valence-band states. Paradoxically, this strong electron-phonon effect which generates the weakly dispersive acoustic surface phonon occurs only because of the highly dispersive character of the electronic surface bands.

The agreement between our calculated phonon energies and the experiment of HTW is qualitative. Phonon energies obtained in our theory can be considered accurate within $\sim 10\%$ (we overestimate the zone-edge TA mode in bulk Si by about 10% ,³⁹ and because of the finite thickness of the slab in the calculations the relative position of the electronic surface bands with respect to the valence-band maximum might also be off by 0.1–0.2 eV in our calculations, affecting the indirect gap that causes the mode softening we discussed here). In the experiment the broad resonance at $\bar{\Gamma}$ is centered at 10.5 meV with FWHM of 3 meV, consistent with our results. At the zone edge the experiment finds two surface phonons with energies 10.5 and 11.5 meV, compared with 12 and 16 meV at \bar{J} and 11 and 15 meV at \bar{K} in our calculations. The experimental width at the possible crossing point (~ 4 meV) does not permit a clear indication whether mode repulsion or crossing occur. The experiment finds a dispersionless model, whereas our results in-

dicating a weakly dispersive one (again, this might be a result of the two remarks made above: our model overestimates the bulk TA phonon at the zone edge and the relative position of the surface states with respect to the valence-band maximum might be off by 0.1–0.2 eV).

Finally, we briefly comment on the rocking mode R , which was not observed in the experiment of HTW. This discrepancy might be related to the fact that the high energy of this branch made it inaccessible in the experiment, where 20–30-meV He atoms were used. Furthermore, one should consider the He-atom activity of each vibration; it is likely that the optical vibration of the surface chains generate a short-wavelength surface corrugation that is not detected by the He atoms, compared with the acoustic mode. It would be interesting to use an atomic charge superposition method to calculate the He-atom activity of each surface vibration.

V. DIPOLE ACTIVITY OF SURFACE PHONONS

In this section we discuss the dipole activity of the surface phonons, or surface conductivity $\sigma_1(\omega)$ of Eq. (26). As we mentioned in the Introduction, we find an unambiguous, though somewhat surprising, explanation for the anomalously strongly dipole-active surface phonon of the Si(111) 2×1 surface seen in EELS experiments. We have previously discussed this result in a short communication,¹ where the on-site electron-repulsion term H_U was not included in our theory; here we expand our discussion, with H_U included in the calculations (the conclusions are essentially the same). The first experimental observation of the strongly dipole-active surface phonon was made by Ibach¹⁶ sixteen years ago, and later experiments have confirmed this result.^{14,24} This dipole-active surface phonon is intrinsic to the 2×1 reconstruction of the Si(111) surface, and its understanding has been a long-standing problem in the vibrational spectroscopy of semiconductor surfaces. Previous theoretical attempts to understand this feature were not related to the π -bonded chain model and did not propose any assignment for the dipole-active surface phonon. Evans and Mills⁴⁰ estimated the size of the dynamic charge of this surface phonon using the intensity of the phonon inelastic peak in the measured EELS spectrum. They calculated $e^* \sim 0.5e - 1.0e$, indeed a very large value for any type of semiconductor structure; they did not, however, provide any microscopic picture of this phenomenon. Previous work by Ludwig,⁴¹ using a force-constant model, speculated that the dipole-active surface phonon arises from the backfolding of the bulk-projected phonons due to the 2×1 reconstruction; he argued, however, that the explanation of this feature might very well depend on the specific structure of the reconstructed surface, and more importantly, on the change of the force constants induced by the reconstruction. The solution of this interesting problem has remained elusive and has been the subject of much speculation. We proposed, for the first time, a microscopic explanation for the anomalously strongly dipole-active surface phonon of Si(111) 2×1 .¹ Our explanation relates the π -bonded chain model to this surface phonon, and this adds to the

long list of evidence in favor of the chain model as the correct model for the reconstruction of Si(111) 2×1 . As we have mentioned, we assign the longitudinal-optical phonon of the surface chains (the dimer mode) as this surface phonon. We have also suggested an experiment that tests this assignment, which has been done and is indeed in agreement with our result.

The calculated phonon-assisted contribution to the surface conductivity $\sigma_1(\omega)$ is shown in Fig. 7, where we plot $\sigma_1(\omega)$ versus phonon energy. The mirror-plane symmetry of the surface (perpendicular to the chain direction) allows us to assign each vibrational mode into one of two representations: (1) even modes, polarized parallel to the mirror plane (i.e., normal to the surface and to the surface chains), and (2) odd modes, polarized along the chain direction (parallel to the surface). The two panels in Fig. 7 follow this symmetry classification [only zone-center phonons enter in the calculation of $\sigma_1(\omega)$, and the mirror plane is in the small group at $\bar{\Gamma}$]. The upper panel shows the dipole activity of all the even modes $\sigma_1^\perp(\omega)$, and the lower panel shows the dipole activity of the odd modes $\sigma_1^\parallel(\omega)$. A phonon that is even under the mirror-plane symmetry drives a current parallel to the mirror plane (the plane defined by $\langle 111 \rangle$ and $\langle 11\bar{2} \rangle$), and a surface vibration that is odd drives a current along the surface chains (parallel to $\langle 1\bar{1}0 \rangle$).

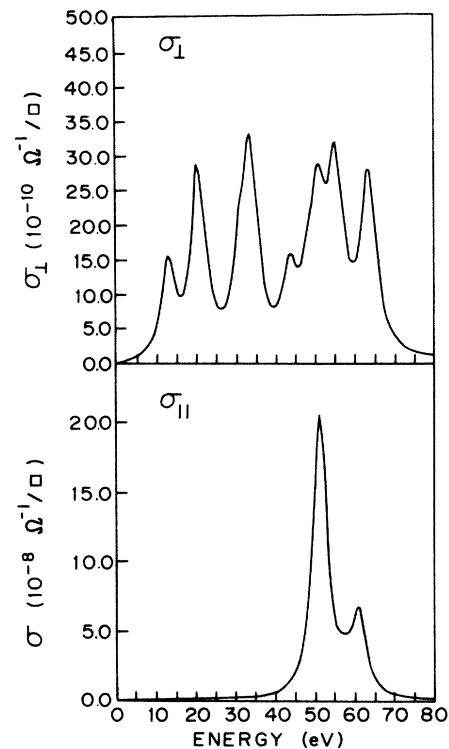


FIG. 7. Surface conductivity (a) $\sigma_1^\perp(\omega)$ polarized perpendicular to the surface chains direction, (b) $\sigma_1^\parallel(\omega)$ polarized parallel to the chains. The continuous spectra are obtained from the original discrete ones by convolution with a Lorentzian with FWHM of 5 meV, comparable to the best available experimental resolution of EELS spectrometers.

The absorption spectrum of the even modes, $\sigma_{\parallel}^+(\omega)$, shows a complex structure, but there is not any particular feature that stands out. We just comment on the broad peak centered near 55 meV. This feature is common to all the Si surfaces we have studied, including the Si(001) surface² and the π -bonded molecular model of Si(111) 2×1 (see the Appendix); it arises from the surface-terminated bulk phonons, which couple to the electronic surface states and the tails of the electronic bulk states in the surface region; the inversion symmetry of crystalline bulk silicon that forbids the dipole activity of the bulk phonons is broken by the surface. The intensity of this broad peak derives from the high density of projected optical bulk phonons in the 50–55-meV region of the spectrum. On the other hand, the spectrum of the odd modes, $\sigma_{\parallel}^-(\omega)$, consists of one sharp peak and a much weaker, also sharp peak on its high-frequency shoulder. The strong peak, positioned at 51 meV, is generated by one phonon: the LO mode of the surface chains. The weaker peak, centered at 61 meV, is the subsurface dimer mode. Note that the vertical scale for $\sigma_{\parallel}^+(\omega)$ is 2 orders of magnitude smaller than the vertical scale for $\sigma_{\parallel}^-(\omega)$, that is, the 51-meV peak in the odd-mode spectrum is more than 100 times larger than the even-mode spectrum.

Thus the picture that emerges from our calculations is that the LO mode of the surface chains completely dominates the one-phonon absorption spectrum of the chain model of the Si(111) 2×1 surface. In our calculations the dynamic charge associated with the dimer mode is $0.75e$, an anomalously large value for homopolar semiconductor structures. This value is consistent with the estimate of Evans and Mills derived from the experiment. The shoulder in $\sigma_{\parallel}^-(\omega)$ due to the subsurface dimer mode and the structure of $\sigma_{\parallel}^+(\omega)$ were not seen in the experiment; they are overshadowed by the strong peak of the LO phonon of the surface chains.

The large charge fluctuations generated by the LO phonon of the surface chains are generated almost entirely by the coupling of the electronic surface states to this mode. This can be seen from Fig. 8, where we plot the surface-state layer-averaged charge density and the layer-averaged dynamic charges e_L^* polarized along the chain direction. e_L^* , where L denotes layer number, is defined as follows:

$$e_L^* = \left[\sum_i (e_i^*)^2 \right]^{1/2}, \quad (31)$$

where the sum is over atoms in layer L . Both quantities decay very quickly into the bulk in a correlated way, showing that the charge fluctuation is almost entirely provided by the response of the surface electrons. Note that close to the center of the slab $e^* \sim 0$, as required by the inversion symmetry in the diamond structure. In Fig. 9 we plot e^* for the three polarizations: normal to the surface, across the chain direction, and parallel to the chain direction. The anisotropy imposed by the surface chains is evident.

In order to understand this result, we look more closely on the effect of the LO phonon of the surface chains on the electronic structure of the surface. Let us consid-

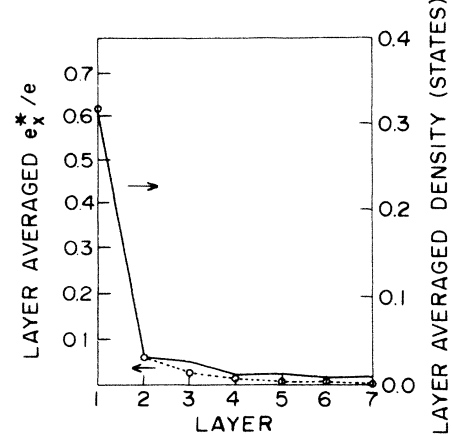


FIG. 8. Filled surface-state layer-averaged charge density and layer-averaged dynamic charge polarized in the chain direction, as a function of penetration depth into the bulk.

er an effective electronic Hamiltonian H^{eff} where we project all the electronic degrees of freedom onto the dangling bond states of the two surface atoms; this will simplify our arguments and will expose the essential physics. We then have an effective one-dimensional chain with two inequivalent sites, corresponding to the two inequivalent surface atoms along the surface chains of Si(111) 2×1 . Let us denote the on-site energies of the two sites ϵ_1 and ϵ_2 , and the effective interaction between electrons in neighboring sites along the chain V_0 . The corresponding k -dependent tight-binding Hamiltonian is

$$H^{\text{eff}} = \begin{bmatrix} \epsilon_1 & V(k) \\ V(k)^* & \epsilon_2 \end{bmatrix}, \quad (32)$$

where the interaction term $V(k)$ is

$$V(k) = V_0(1 + e^{ika}), \quad (33)$$

k is the corresponding Bloch wave vector, and a is the length of the unit cell. Consider how vibrations of the chains affect H^{eff} . If the TA optical mode of the chains, the rocking mode, is excited, the on-site energies change:

$$\begin{aligned} \epsilon_1 &\rightarrow \epsilon_1 + \Delta \cos(\omega t), \\ \epsilon_2 &\rightarrow \epsilon_2 - \Delta \cos(\omega t), \end{aligned}$$

where ω is the phonon frequency. Charge is transferred up and down along a bond between the two surface atoms. If the LO mode of the chains, the dimer mode, is excited, the interaction V is changed:

$$V \rightarrow V + \delta V \cos(\omega t),$$

the perturbation is on the off-diagonal part of H^{eff} , and the entire electronic structure changes; charge not only fluctuates along a bond between nearest neighbors, but along the entire chain. The LO phonon of the surface chains couples very efficiently to the states across the gap at the zone edge. Two crucial properties of the sur-

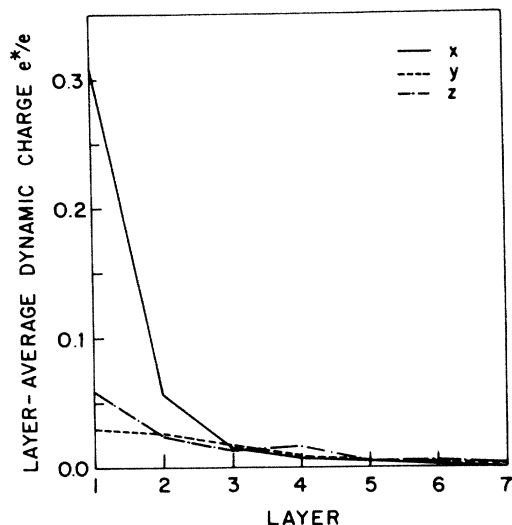


FIG. 9. Layer-averaged dynamic charges polarized along the chain direction (solid line), normal to the surface plane (dashed line), and perpendicular to the chain direction, parallel to the surface plane (dash-dotted line).

face contribute so that the LO mode of the chains can drive a very large charge fluctuation: first of all, the electrons along the chains are delocalized, and it is easy then to generate a charge fluctuation; and second, a connected network of surface atoms exists that can support the charge oscillations without interruption. This is in sharp contrast to the Si(001) surface, where there is no such connected network of surface atoms and most of the phonon-induced charge fluctuations occur through the back bonds.²³

We assign the LO mode of the surface chains as the Si(111) 2×1 surface phonon seen in EELS experiments. The frequency of this phonon in our calculations is 51 meV; experimentally it is found around 56 meV.^{16,14} Notice that this mode is odd with respect to the mirror-plane symmetry, and therefore its dynamic dipole is polarized along the chains parallel to the surface. This violates the so-called dipole-selection rule,¹⁷ which states that only perpendicular dipoles can occur on a surface. However, this selection rule is valid for ideal metallic screening, where the static dielectric constant diverges. On a semiconductor or an insulator surface, where there is a gap in the electronic bands, the dipole-selection rule can break down. We should point out here that our model includes short-range, but no long-range electrostatic screening, thus we probably overestimate the magnitude of the dynamic charges. The calculated dielectric constant that we obtain (short-range screening) is $\epsilon(\mathbf{q}=0)=14$, compared to its experimental value of 12. The interesting property of the LO phonon of the chains, that its dynamic dipole is polarized parallel to the chain direction, can be used to test our assignment. In an azimuthal angle-dependent EELS experiment, when the surface chains project onto the scattering plane, the inelastic spectrum should be dominated by a single sharp and strong peak near 51 meV, but as the scattering plane is rotated this signal should quench and

should disappear when the scattering plane is perpendicular to the surface chains, provided that the experiment is done on a single domain surface (with a unique chain direction). This is the vibrational analogue to the experiments by Chiradia *et al.*³⁴ and by Olmstead and Amer,³⁵ where the polarization dependence of the optical absorption of the electronic surface states was measured. In both of these cases a $\cos^2\phi$ behavior, where ϕ is the azimuthal angle, was observed, confirming the existence of the quasi-one-dimensional surface chains and the mirror-plane symmetry of the surface. An interesting electron-scattering experiment has been recently reported by DiNardo *et al.*,¹⁴ and our prediction was confirmed. This was the first experimental observation of a parallel dynamic dipole on a clean surface. The analysis of the experiment, however, is unfortunately not as easy as in the optical case; the lower resolution of electron scattering compared to optical absorption, and the small q transfer of the EELS process, make a detailed analysis of the effects of angle resolution in the experimental data necessary. For finite sizes in the collection angles of the spectrometer, the $\cos^2\phi$ result of the optical-absorption experiments becomes less sharp in the EELS experiments, and the signal does not completely vanish in the perpendicular geometry (see Ref. 42).

VI. SUMMARY

We have studied vibrational properties of the π -bonded chain model of the Si(111) 2×1 surface using a theory of vibrational excitations that is based on an empirical tight-binding model for structural energies in Si. This is a simple theory that is nevertheless capable of incorporating the surface electrons into the formulation of the dynamical properties of the surface. We have calculated surface-phonon dispersion relations, and the phonon-assisted contribution to the surface conductivity, or dipole activity of surface phonons. We find, in general, that the vibrational properties of Si(111) 2×1 are radically different than in the bulk, and just as the zig-zag chains of the reconstructed surface determine its electronic properties, the vibrational properties of the surface are also characteristic of the chain geometry. An important conclusion of our studies is that the surface electrons play a fundamental role in the lattice dynamics of the surface; the delocalization of the surface electrons along the surface chains is the signature of the chain model of the reconstruction of the surface, and these quasi-one-dimensional surface electrons strongly influence the surface lattice dynamics. Our calculation of the surface dynamic charges demonstrates this; we assign a longitudinal-optical phonon along the surface zig-zag chains, a mode that dimerizes them, as the anomalously strongly dipole-active surface phonon seen in EELS. The dynamic charge generated by this vibration is extremely large, $\sim 0.75e$, and has the novel property that is polarized parallel to the surface plane, along the chain direction. This property can be used to test our assignment, and a recent experiment has shown that the longitudinal-optical mode of the chains is indeed the anomalously strongly dipole-active Si(111) 2×1 surface

phonon. The explanation of this feature had been a long-standing problem in the vibrational spectroscopy of semiconductor surfaces. Another unique vibrational property of the Si(111) 2×1 surface where the electrons play a central role is the appearance of a low-energy acoustic surface phonon with almost no dispersion. The recent experimental observation of this surface phonon raised the question of whether the π -bonded chain model could explain this feature of an Einstein-like vibration, or whether an alternative reconstruction of the surface, where localized vibrations can occur, ought to be considered. We find that our calculated phonon spectrum is in qualitative agreement with the experiment, and that the dispersionless character of this vibration results from a strong phonon-energy renormalization effect due to virtual transitions from the back-bond states to the zone-edge empty surface states, a subsurface-mediated effect. Even though both surface electrons and surface phonons are very well localized on the surface itself, one cannot regard this surface as completely decoupled from the bulk. The dispersion of the surface phonons demonstrates that the force constants at the surface are very different from the bulk; in order to accurately describe the vibrational properties of the surface, one has to calculate them, and not merely use bulk force constants, and one has to include the effect of the surface electrons.

ACKNOWLEDGMENTS

This work was supported by the U.S. Department of Energy under Grant No. DE-FG02-84ER45118. We thank Dr. Douglas Allan for a critical reading of the manuscript.

APPENDIX: THE π -BONDED MOLECULAR MODEL

The π -bonded molecular model was proposed by Chadi²⁵ as an alternative model for the reconstruction of the Si(111) 2×1 surface. The motivation for this was that Pandey's π -bonded chain model could not apparently explain some conflicting results reported from angle-resolved photoemission experiments. Uhrberg *et al.*¹⁰ found one occupied surface band with large upward dispersion in the $\bar{\Gamma}$ to \bar{J} direction, in agreement with the π -bonded chain model. Himpsel *et al.*⁹ found, besides the highly dispersive surface band characteristic of the π -bonded chain model, a second weakly dispersive band at lower energies, inside the valence-band region. Houzay *et al.*⁴³ found different results for differently prepared surfaces, depending on the cleavage direction relative to the 2×1 reconstruction; in some of these surfaces they found only a flat surface band. Since these initial experiments were reported, the appearance of the second, weakly dispersive surface band has been interpreted as arising from multidomain surfaces or from transitions from the bulk valence bands to the unoccupied surface states of the chain model, and for single domain 2×1 surfaces only the strongly dispersive band of the π -bonded chain model is observed. No further evidence in support of the molecular model has been found. Theoretically, total-energy calculations⁴⁴ show that the chain model has lower energy than the molecu-

lar model by ~ 0.3 eV/surface atom, a relatively large amount.

Even though there is no single clear experiment in favor of the molecular model, and there is overwhelming evidence in support of the chain model, it is worthwhile from the theoretical point of view to compare these two models. Specifically, we are interested here in comparing their phonon excitation spectra. We find that the π -bonded molecular model does not support a strongly dipole-active surface phonon in agreement with the EELS results.

The reconstructed geometries of the chain and the molecular models are completely different. In the chain model the surface atoms form strongly bonded zigzag chains, a connected network of surface atoms, whereas in the molecular model the surface atoms form isolated dimers. The surface geometry of the molecular model is somewhat similar to the Si(001) 2×1 surface, and indeed their electronic surface bands are also similar.⁴⁴ The molecular model does not have a mirror-plane symmetry normal to the $\langle 1\bar{1}0 \rangle$ direction, which is the direction of the chains in the chain model; the existence of this surface symmetry has been confirmed experimentally.³⁴⁻³⁶

We have calculated the equilibrium structure, the zone-center phonons, and the phonon-absorption spectrum of the π -bonded molecular-model surface. The phonon-absorption spectrum is shown in Fig. 10. We show separately the component perpendicular to the $\langle 1\bar{1}0 \rangle$ direction $\sigma_{\perp}^{\parallel}(\omega)$, and the parallel component $\sigma_{\parallel}^{\parallel}(\omega)$. If \hat{x} , \hat{y} , and \hat{z} denote the directions $\langle 1\bar{1}0 \rangle$, $\langle 11\bar{2} \rangle$, and $\langle 111 \rangle$, respectively, then $\sigma_{\perp}^{\parallel}(\omega) = \sigma_y(\omega) + \sigma_z(\omega)$ and $\sigma_{\parallel}^{\parallel}(\omega) = \sigma_x(\omega)$. Figure 10 can then be directly compared with the corresponding figure for the π -bonded chain model (Fig. 7). There are three main

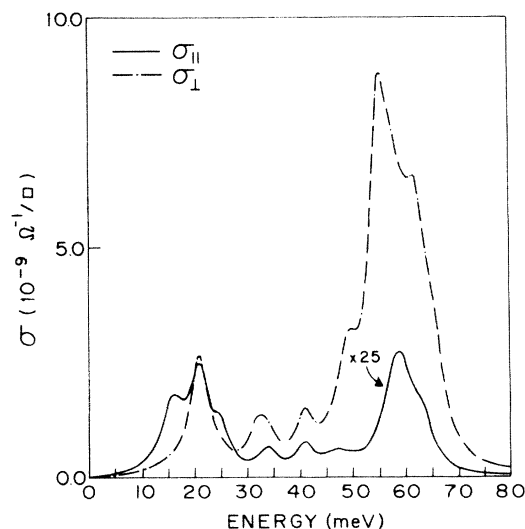


FIG. 10. Surface conductivity of the π -bonded molecular model, $\sigma_{\parallel}^{\parallel}(\omega)$ is polarized along the chain direction of the chain model ($\langle 1\bar{1}0 \rangle$), and $\sigma_{\perp}^{\parallel}(\omega)$ is polarized normal to the chain direction. Notice that $\sigma_{\parallel}^{\parallel}$ is multiplied by a factor of 25. This figure can be directly compared with the corresponding figure for the chain model, Fig. 7.

points of disagreement between the phonon-absorption spectrum of the molecular model, and the experimental results.

(1) The phonon-absorption spectrum of the molecular model does not have a single sharp peak that dominates the entire spectrum. Its strongest feature is a broad peak centered at ~ 55 meV, and has a second weaker and also broad peak centered at ~ 20 meV. The phonon-absorption spectrum of the chain model has one sharp peak at 51 meV (with a weak subpeak at 60 meV) that is generated by the LO phonon of the surface chains and completely dominates the absorption spectrum. The results of EELS experiments^{16,14} show a single, very sharp absorption peak at ~ 56 meV.

(2) The intensity of the strongest feature in this spectrum is ~ 50 times weaker than the absorption peak of

the LO mode of the surface chains; the molecular model does not support a surface phonon that can drive a large dynamic charge comparable with experiment ($e^* = 0.5 - 1.0e$).

(3) Note that $\sigma_{\parallel}(\omega)$ is scaled 25 times in the figure, that is, almost all the dipole activity in the molecular model is polarized normal to the $\langle 1\bar{1}0 \rangle$ direction, and furthermore most of the strength in $\sigma_{\perp}(\omega)$ comes from the \hat{z} polarization, normal to the surface. No azimuthal angle dependence of the absorption spectrum should be observed. The experiment of DiNardo *et al.*¹⁴ shows that there is an azimuthal angle dependence that implies that the Si(111) 2×1 dipole-active surface phonon is polarized along the $\langle 1\bar{1}0 \rangle$ direction, consistent with our assignment of this phonon as the LO vibrations of the surface chains.

- *Present address: Department of Physics, (Room 12-110) Massachusetts Institute of Technology, Cambridge, MA 02139.
- ¹O. L. Alerhand, D. C. Allan, and E. J. Mele, *Phys. Rev. Lett.* **55**, 2700 (1985).
- ²O. L. Alerhand and E. J. Mele, *Phys. Rev. Lett.* **59**, 657 (1987).
- ³K. C. Pandey, *Phys. Rev. Lett.* **47**, 1913 (1981); **49**, 233 (1982).
- ⁴J. E. Northrup and M. L. Cohen, *Phys. Rev. Lett.* **49**, 1349 (1982); *J. Vac. Sci. Technol.* **21**, 333 (1982); *Phys. Rev. B* **27**, 6553 (1983).
- ⁵R. M. Feenstra, W. A. Thompson, and A. P. Fein, *Phys. Rev. Lett.* **56**, 608 (1986).
- ⁶J. A. Stroschio, R. Feenstra, and A. P. Fein, *Phys. Rev. Lett.* **57**, 2579 (1986).
- ⁷R. M. Tromp, L. Smit, and J. F. van der Veen, *Phys. Rev. Lett.* **51**, 1672 (1983); *Phys. Rev. B* **30**, 6235 (1984).
- ⁸F. J. Himpsel, P. M. Marcus, R. Tromp, I. P. Batra, M. R. Cook, F. Jona, and H. Liu, *Phys. Rev. B* **30**, 2257 (1984).
- ⁹F. J. Himpsel, P. Heimann, and D. E. Eastman, *Phys. Rev. B* **24**, 2003 (1981).
- ¹⁰R. I. G. Uhrberg, G. V. Hansson, J. M. Nicholls, and S. A. Flodström, *Phys. Rev. Lett.* **48**, 1032 (1982).
- ¹¹D. Straub, L. Ley, and F. J. Himpsel, *Phys. Rev. Lett.* **54**, 142 (1985).
- ¹²P. Martensson, A. Cricenti, and G. V. Hansson, *Phys. Rev. B* **32**, 6959 (1985).
- ¹³H. Lüth, A. Ritz, and R. Matz, *Solid State Commun.* **46**, 343 (1983).
- ¹⁴N. J. DiNardo, W. A. Thompson, A. J. Schell-Sorokin, and J. E. Demuth, *Phys. Rev. B* **32**, 3007 (1986).
- ¹⁵G. Chiarotti, S. Nannarone, R. Pastore, and P. Chiradia, *Phys. Rev. B* **4**, 3398 (1971).
- ¹⁶H. Ibach, *Phys. Rev. Lett.* **27**, 253 (1971).
- ¹⁷H. Ibach and D. L. Mills, *Electron Energy Loss Spectroscopy and Surface Vibrations* (Academic, New York, 1982).
- ¹⁸U. Harten, J. P. Toennies, and Ch. Wöll, *Phys. Rev. Lett.* **57**, 2947 (1986).
- ¹⁹D. J. Chadi, *Phys. Rev. Lett.* **41**, 1062 (1978).
- ²⁰C. M. Varma and W. Weber, *Phys. Rev. Lett.* **38**, 1094 (1977); *Phys. Rev. B* **19**, 6142 (1979).
- ²¹W. Weber, in *The Electronic Structure of Complex Systems*, Vol. 113 of *NATO Advanced Study Institute, Series B: Physics*, edited by P. Phariseau and W. M. Temmerman (Plenum, New York, 1984), p. 345.
- ²²D. H. Lee and J. D. Joannopoulos, *Phys. Rev. Lett.* **48**, 1846 (1982).
- ²³O. L. Alerhand and E. J. Mele, *Phys. Rev. B* **35**, 5533 (1987).
- ²⁴J. A. Schäfer, J. Anderson, and P. J. Lapeyre, *J. Electron Spectrosc. Rel. Phenom.* **38**, 21 (1986).
- ²⁵D. J. Chadi, *Phys. Rev. B* **26**, 4762 (1982).
- ²⁶D. J. Chadi, *Phys. Rev. Lett.* **43**, 43 (1979).
- ²⁷W. A. Harrison, *Electronic Structure and Properties of Solids* (Freeman, San Francisco, 1980), p. 48.
- ²⁸M. Cardona, in *Light Scattering in Solids II*, Vol. 50 of *Topics in Applied Physics*, edited by M. Cardona and G. Güntherodt (Springer-Verlag, New York, 1982), p. 58.
- ²⁹R. M. Tromp, L. Smit, and J. F. van der Veen, *Phys. Rev. Lett.* **51**, 1672 (1983).
- ³⁰G. Chiarotti, S. Nannarone, R. Pastore, and P. Chiradia, *Phys. Rev. B* **4**, 3398 (1971); P. Chiradia, A. Cricenti, S. Selci, and G. Chiarotti, *Phys. Rev. Lett.* **52**, 1145 (1984); M. A. Olmstead, and N. M. Amer, *ibid.* **52**, 1148 (1984); N. J. DiNardo, J. E. Demuth, W. A. Thompson, and Ph. Avouris, *Phys. Rev. B* **31**, 4077 (1985); J. A. Stroschio, R. M. Feenstra, and A. P. Fein, *Phys. Rev. Lett.* **57**, 2579 (1986).
- ³¹R. M. Tromp, L. Smit, and J. F. van der Veen, *Phys. Rev. B* **30**, 6235 (1984).
- ³²F. J. Himpsel, P. Heimann, T.-C. Chiang, and D. E. Eastman, *Phys. Rev. Lett.* **45**, 1112 (1980).
- ³³K. C. Pandey, *Phys. Rev. Lett.* **47**, 1913 (1981).
- ³⁴P. Chiradia, A. Cricenti, S. Selci, and G. Chiarotti, *Phys. Rev. Lett.* **52**, 1145 (1984).
- ³⁵M. A. Olmstead and N. M. Amer, *Phys. Rev. Lett.* **52**, 1148 (1984).
- ³⁶T. F. Heinz, M. M. T. Loy, and W. A. Thompson, *Phys. Rev. Lett.* **54**, 63 (1985).
- ³⁷D. C. Allan and E. J. Mele, *Phys. Rev. Lett.* **53**, 826 (1984).
- ³⁸The Rayleigh wave is found off the bottom of the acoustic continuum.
- ³⁹E. J. Mele, D. C. Allan, O. L. Alerhand, and D. P. DiVincenzo, *J. Vac. Sci. Technol. B* **3**, 1068 (1985).
- ⁴⁰E. Evans and D. L. Mills, *Phys. Rev. B* **5**, 4126 (1972).
- ⁴¹Wolfgang E. W. Ludwig, *Jpn. J. Appl. Phys., Suppl. 2*, **2**, 879 (1974).
- ⁴²O. L. Alerhand, N. J. DiNardo, and E. J. Mele, *Surf. Sci.* **173**, L659 (1986).
- ⁴³F. Houzay, G. Guichar, R. Pinchaux, G. Jezequel, F. Solal, A. Barski, P. Steiner, and Y. Petroff, *Surf. Sci.* **132**, 40 (1983).
- ⁴⁴O. H. Nielsen, Richard M. Martin, D. J. Chadi, and K. Kunc, *J. Vac. Sci. Technol. B* **1**, 714 (1983).